International Journal of Fracture manuscript No.
(will be inserted by the editor)

A fast algorithm for the elastic fields due to a single fiber break in a periodic fiber-reinforced composite

Ankit Gupta, Sivasambu Mahesh, Shyam M. Keralavarma

Received: date / Accepted: date

Abstract The stress state in a shear-lag model of a unidirectional linear fiber composite with an arbitrary configuration of fiber breaks is obtained by the weighted superposition of the stress state due to a single broken fiber. In a periodic patch comprised of N fibers located at the points of a regular lattice, a method to determine the stress state due to a single break was proposed by Landis et al., Micromechanical simulation of the failure of fiber reinforced composites. Journal of the Mechanics and Physics of Solids 2000; 48(3):621–648. This method entails the determination of the eigenspace of an $N \times N$ matrix, at a computational cost of $O(N^3)$. In the present work, an alternative algorithm is proposed. This algorithm exploits the circulant structure of the matrix describing the inter-fiber interactions. The asymptotic computational complexity of the present algorithm equals that of the discrete Fourier transform: $O(N \log\ N)$. Run times of the present method with the eigensolution based method are compared, and shown to be very favorable for the present method, even for small N. Power-law scaling of the overloads due to a single break to much larger distances than previously possible has been verified using the present method.

Keywords Composites; Fracture; Discrete Fourier Transform; Lattice models; Circulant matrix; Periodic boundary condition

1 Introduction

The ultimate tensile strength of fiber reinforced polymer matrix composites shows wide scatter. This derives from the stochastic variability in the strength of the fibers (Hull and Clyne 1996). Monte-Carlo simulations of composite failure are a fruitful approach (Smith 1980; Beyerlein et al 1996; Zhou and Curtin 1995; Curtin 1998; Landis et al 2000; Mahesh et al 1999, 2002; Mahesh and Phoenix 2004) to understand the relationship between the strength distribution of the fiber, and that of the composite. In this approach, the failure of a composite comprised of N fibers, whose strengths are drawn from a known probability distribution are simulated on a computer. From an initial break-free state, the computer fibers are sequentially broken when the load carried by them exceeds their random strength. Load is redistributed amongst the surviving fibers at each stage following a load sharing law.

Repeated simulation with different realizations of fiber strengths drawn from the same probability distribution yields a computer-generated empirical strength distribution for the composite. This can be used to validate stochastic models of composite fracture, and scaling laws for composite strength with the number of fibers, N (Smith 1980; Curtin 1998; Mahesh et al 2002). Monte-Carlo studies that are substantially similar to those involving fiber composites have also been used to understand the breakdown of random fuse networks (De Arcangelis et al 1985; Duxbury and Leath 1987), and in earthquake studies (Newman et al 1994).

A shear-lag model for a composite comprised of $N = \infty$ fibers was proposed for one- and two-dimensional patches by Hedgepeth (1961) and Hedgepeth and Van Dyke (1967), respectively. These authors also determined an analytical solution for the single break problem upto numerical quadrature of a rapidly oscillating integrand. Their solutions are, however, not suitable for Monte-Carlo simulations, which must necessarily be performed on finite patches. Using the $N = \infty$, Hedgepeth (1961)

Ankit Gupta · Sivasambu Mahesh (✉) · S. M. Keralavarma
Department of Aerospace Engineering, Indian Institute of Technology Madras, Chennai 600 036, India.
E-mail: smahesh@iitm.ac.in

or Hedgepeth and Van Dyke (1967) solutions in a finite patch simulation causes a part of the load dropped by a broken fiber in the patch to be transferred to fibers outside the patch. Therefore the net patch load in such simulations is not conserved with increasing number of fiber breaks. This renders the empirical strength distributions obtained from such simulations unrealistic.

An elegant method to overcome the problem of lost load was proposed by Landis et al (2000). By imposing periodic boundary conditions on their N-fiber patch, they ensured conservation of the net load therein. Their solution methodology involves the eigensolution of an $N \times N$ interaction matrix; the single break solution is obtained as a weighted superposition of the N eigenvectors.

Computationally, the most intensive parts of a Monte-Carlo failure simulation in a composite obeying an elastic shear-lag model are (i) the determination of the single break solution, and (ii) the determination of the stress concentration due to the current set of breaks, in order to determine the next new break. Calculation (i) represents a one time analysis performed prior to the failure simulations, while (ii) is performed at each stage of the simulations. The focus of the present work is on an algorithm for substantially speeding up (i).

It is presently only feasible to perform Monte-Carlo simulations on patches that are much smaller than realistic composites. In such simulations, even with periodic boundary conditions (Landis et al 2000), patch size effects can obscure the connection between the empirical strength distribution obtained from Monte Carlo simulations, and the strength distribution of the realistic composite. For example, from simulations of composite patches comprised of upto $N = 900$ fibers, Mahesh et al (2002) found that at large fiber Weibull moduli, the empirical strength distribution clearly displayed a weakest-link scaling character. With decreasing fiber Weibull modulus, they found that the composite strength distribution approached the normal distribution. Simultaneously, the cluster of breaks at the point of fracture became comparable to the patch size. It was thus not clear if the qualitative switch in the character of the empirical composite strength distribution was caused by decreasing Weibull modulus, or was merely an artifact due to the limited patch size. As another example, Curtin (1998) proposed that the composite strength distribution follows a weakest-link structure, with the weakest link obeying the normal distribution. He validated this model using Monte-Carlo simulations for patch sizes up to $N = 2500$. In another study assuming local load sharing, Habeeb and Mahesh (2015) found that Curtin's scaling could explain the Monte-Carlo generated empirical strength distributions in patches comprised of a few thousand fibers well. The agreement, however, ceased when applied to Monte-Carlo generated empirical strength distributions from larger patches comprised of $N = 10^5$ fibers.

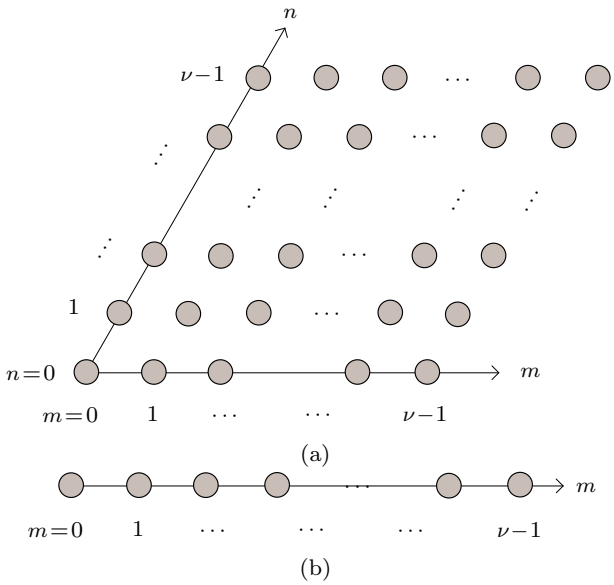

Fig. 1: (a) A rhombus-shaped periodic patch of $\nu \times \nu$ fibers arranged in a hexagonal lattice showing the m–n coordinate system (Sec. 2.1). (b) A linear periodic patch of ν fibers showing the m coordinate system (Sec. 2.5).

It is clear from the foregoing example that it may be necessary to perform Monte-Carlo simulations using patches comprised of orders of magnitude more fibers than in the aforementioned literature. One impediment to this is the determination of the single break solution for large N following Landis et al (2000), on account of the $O(N^3)$ complexity of eigenspace extraction. In the present work, an alternative algorithm based on the discrete Fourier transform (DFT) and involving only $O(N \log\ N)$ computational effort is proposed. The present algorithm is much faster: for example, it yields the solution for the unit break problem for an $N = 2^{20} \approx 10^6$ patch, in less than one second on a workstation computer.

2 Model and algorithm

2.1 Governing equations

A rhombus-shaped finite 'patch' comprised of $N = \nu^2$ fibers arranged in a hexagonal lattice is taken to represent the cross-section of the unidirectional composite. This patch is depicted in Fig. 1 (a). The greatest fiber volume fraction is obtained when fibers are located at the points of a regular close packed lattice. Accordingly,

fibers are assumed to occupy the points of a hexagonal lattice in Fig. 1 (a). Two edges of the rhombus define the m, and n coordinate axes. The following periodicity conditions are imposed: fibers $(0, n)$ and $(\nu-1, n)$ (the left and right edges of the patch) are assumed adjacent for all $n \in \{0, 1, \ldots, \nu-1\}$. Similarly, fibers at the top $(n = \nu-1)$ and bottom $(n = 0)$ edges are also considered adjacent. On account of periodicity, only fiber indices modulo ν are significant. For any integer a, these are defined as

$$[a] := a - \nu \lfloor a/\nu \rfloor . \tag{1}$$

Here, $\lfloor a/\nu \rfloor$ denotes the largest integer no greater than a/ν.

Hedgepeth (1961) showed that by suitably non- dimensionalizing the fiber-wise positional coordinate, and the axial displacements, the governing equations may be freed of all material parameters, in the linear elastic case. This approach has been adopted in the literature since (Hedgepeth and Van Dyke 1967; Mahesh et al 1999; Landis et al 2000). Let $u_{mn}(\zeta)$ denote the normalized displacement of fiber (m, n) in the fiber direction, at normalized fiber-wise positional coordinate, ζ. The governing equilibrium equations along the fiber direction, in Hedgepeth's framework are

$$\frac{d^2 u_{mn}}{d\zeta^2}(\zeta) + A_{mnpq} u_{pq}(\zeta) = 0. \tag{2}$$

Here and elsewhere, summation over repeated Latin indices over the range $\{0, 1, \ldots, \nu-1\}$ is implied, unless otherwise noted. Let all the fibers, except the one at $(0, 0)$ be intact. The boundary conditions corresponding to unit normalized opening displacement at the broken fiber, and no displacement of the intact fibers are expressed as

$$u_{mn}(\zeta = 0) = \begin{cases} 1, & \text{if } m = n = 0, \\ 0, & \text{otherwise.} \end{cases} \tag{3}$$

The fourth-order constant coefficient matrix A_{mnpq} in Eq. (2) contains information about interactions between fibers. Zero values of A_{mnpq} indicate no interaction between fibers (m, n) and (p, q), while non-zero values indicate direct interaction. It is assumed that A_{mnpq} satisfies the translation invariance property, viz.,

$$A_{mnpq} = A_{[m-a],\,[n-b],\;[p-a],\,[q-b]}, \tag{4}$$

where $[\cdot]$ is defined in Eq. (1). This implies that the governing equations are translation invariant with respect to arbitrary lattice translations (a, b). In particular, if the displacement field u_{mn} due to a break located at $(0, 0)$ were available, the displacement field induced by a fiber break located at (a, b) would simply be $u_{[m-a],[n-b]}$.

The following interaction matrix, which represents interactions of each fiber with its first ring of neighbors (Hedgepeth and Van Dyke 1967), satisfies the translation invariance property, Eq. (4):

$$A_{mnpq} = \begin{cases} -6, & \text{if } p = m, \text{ and } q = n, \\ 1, & \text{if } p = [m \pm 1], \text{ and } q = n, \\ 1, & \text{if } p = m, \text{ and } q = [n \pm 1], \\ 1, & \text{if } p = [m \pm 1], \text{ and } q = [n \mp 1], \\ 0, & \text{otherwise.} \end{cases} \tag{5}$$

2.2 Diagonalization of the interaction matrix

The fast algorithm proposed in the present work to solve Eq. (2) hinges on the observation that the fourth order matrix A_{mnpq} is circulant along two disjoint pairs of modes, following the terminology of Rezghi and Eldén (2011). Consider the second order matrix A_{MnPq}, obtained by fixing $m = M$, and $p = P$, for some $0 \leq M, P \leq \nu-1$. Then, following the definition of Rezghi and Eldén (2011, Def. (4.2)), Eq. (4) implies that A_{MnPq} is circulant in the pair of modes $\{2, 4\}$, as it satisfies the property:

$$A_{MnPq} = A_{Mn'Pq'}, \quad \text{if } [n-q] = [n'-q'] \tag{6}$$

Similarly, it can be shown that A_{mNpQ} obtained by fixing $n = N$ and $q = Q$ for some $0 \leq N, Q \leq \nu-1$, is also circulant in the pair of modes $\{1, 3\}$.

Circulant matrices, A_{MnPq} and A_{mNpQ}, can be diagonalized by the unitary Fourier matrix Davis (2012), F_ν. In terms of $\omega_\nu = \exp(2\pi i/\nu)$, the Fourier matrix is defined as

$$F_\nu = \frac{1}{\sqrt{\nu}} \begin{pmatrix} 1 & 1 & 1 & \ldots\ldots & 1 \\ 1 & \omega_\nu & \omega_\nu^2 & \ldots\ldots & \omega_\nu^{\nu-1} \\ 1 & \omega_\nu^2 & \omega_\nu^4 & \ldots\ldots & \omega_\nu^{2(\nu-1)} \\ \ldots & \ldots & \ldots & \ldots\ldots & \ldots \\ \ldots & \ldots & \ldots & \ldots\ldots & \ldots \\ 1 & \omega_\nu^{\nu-1} & \omega_\nu^{2(\nu-1)} & \ldots\ldots & \omega_\nu^{(\nu-1)^2} \end{pmatrix}. \tag{7}$$

Numbering the rows and columns in the range $i, j \in \{0, 1, \ldots, \nu-1\}$, it is clear from Eq. (7) that $F_{\nu;\,ij} = \omega_\nu^{ij}/\sqrt{\nu}$.

Rezghi and Eldén (2011, Theorem 5.2) have shown that the higher order matrix A_{mnpq} can also be diagonalized in the disjoint modes $\{1, 3\}$ and $\{2, 4\}$. Thus, if $\overline{F}_{\nu;ij}$ denotes the complex conjugate of $F_{\nu;ij}$,

$$\begin{aligned} D_{abcd} &= \overline{F}_{\nu;am}\, \overline{F}_{\nu;bn}\;\; A_{mnpq}\;\; F_{\nu;pc}\, F_{\nu;qd} \\ &= \omega_\nu^{-am}\, \omega_\nu^{-bn}\;\; A_{mnpq}\;\; \omega_\nu^{pc}\, \omega_\nu^{qd}/\nu^2 \end{aligned} \tag{8}$$

represents a diagonal matrix, whose potentially non-zero diagonal entries are

$$\begin{aligned} D_{abab} &= \nu F_{\nu;am} F_{\nu;bn} A_{mn00}, \\ &= \omega_\nu^{am}\, \omega_\nu^{bn}\ A_{mn00}. \end{aligned} \tag{9}$$

2.3 Solution of the governing equations

Following Briggs and Henson (1995, p. 146), the two-dimensional discrete Fourier transform of $u_{mn}(\zeta)$ is defined as

$$U_{rs}(\zeta) = \frac{1}{\nu^2} u_{mn}(\zeta) \omega_\nu^{-mr} \omega_\nu^{-ns}. \tag{10}$$

Its inverse is given by Briggs and Henson (1995, p. 146),

$$u_{mn}(\zeta) = U_{rs}(\zeta) \omega_\nu^{mr} \omega_\nu^{ns}. \tag{11}$$

Premultiplying Eq. (2) by $\omega_\nu^{-mj}\omega_\nu^{-nk}/\nu^2$, and using Eq. (10) in the first term yields

$$\frac{d^2 U_{jk}}{d\zeta^2}(\zeta) + \frac{1}{\nu^2}\omega_\nu^{-mj}\omega_\nu^{-nk} A_{mnpq} u_{pq}(\zeta) = 0. \tag{12}$$

Substituting Eq. (11) into the second term results in

$$\frac{d^2 U_{jk}}{d\zeta^2}(\zeta) + \frac{1}{\nu^2}\omega_\nu^{-mj}\omega_\nu^{-nk} A_{mnpq}\, \omega_\nu^{pr}\omega_\nu^{qs} U_{rs}(\zeta) = 0. \tag{13}$$

The coefficient matrix in the second term has been obtained previously in Eq. (8). Substituting that expression in Eq. (2) yields

$$\frac{d^2 U_{jk}}{d\zeta^2}(\zeta) + D_{jkrs} U_{rs}(\zeta) = 0. \tag{14}$$

The simplification effected in going from Eq. (2) to Eq. (14) is that D_{jkrs} in the latter equation is diagonal in modes $\{1,3\}$ and $\{2,4\}$. In other words, $D_{jkrs} = 0$, unless $j = r$ and $k = s$. Substituting the boundary conditions corresponding to the single break problem in Eq. (3) into Eq. (10) gives the following boundary conditions in Fourier space

$$U_{jk} = \frac{1}{\nu^2}, \quad \forall j,k \in \{0,1,\ldots,\nu-1\}. \tag{15}$$

For visualization as second-order matrices and vectors, consider the contracted indices: $\alpha = j + k\nu$, and $\beta = r + s\nu$. Denoting $\hat{U}_\alpha = U_{jk}$, $\hat{U}_\beta = U_{rs}$, and $\hat{D}_{\alpha\beta} = D_{jkrs}$, $\alpha,\beta \in \{0,1,\ldots,\nu^2-1\}$, Eq. (14) can be written as

$$\frac{d^2 \hat{U}_\alpha}{d\zeta^2} + \hat{D}_{\alpha\beta}\hat{U}_\beta = 0. \tag{16}$$

Here, repeated Greek indices imply summation over the range $\{0,1,\ldots,\nu^2-1\}$. The boundary conditions Eq. (15) become

$$\hat{U}_\alpha(\zeta = 0) = 1/\nu^2, \quad \forall \alpha \in \{0,1,\ldots,\nu^2-1\}. \tag{17}$$

$\hat{D}$ is a diagonal matrix: $\hat{D}_{\alpha\beta} = 0$, unless $\alpha = \beta$. Its eigenvalues are its diagonal elements and its eigenvectors are the unit vectors along each of the ν^2 coordinate axes. Eq. (16) therefore represents an uncoupled system of ν^2 second-order equations. The solution to the present system of equations that remains bounded at $\zeta = \infty$ is

$$\hat{U}_\alpha = c_\alpha \exp\left(-\sqrt{-\hat{D}_{\alpha\alpha}}\zeta\right), \tag{18}$$

where no summation over α is to be assumed in the right hand side. The scalars c_α are easily determined using the boundary conditions, Eq. (17):

$$c_\alpha = 1/\nu^2, \quad \forall \alpha \in \{0,1,\ldots,\nu^2-1\}. \tag{19}$$

Substituting Eq. (19) into Eq. (18) yields a closed-form displacement solution in Fourier space:

$$\hat{U}_\alpha(\zeta) = \exp\left(-\sqrt{-\hat{D}_{\alpha\alpha}}\zeta\right)/\nu^2. \tag{20}$$

$U_{jk}(\zeta) = \hat{U}_\alpha(\zeta)$ represents the solution for the normalized displacement in Fourier space. Straightforward differentiation with respect to ζ yields the strain in Fourier space. Inverse discrete Fourier transformation using Eq. (11) will yield the displacement and strain fields in physical space. The stress concentration in fiber (m,n) is then (Hedgepeth 1961):

$$K_{mn} := 1 - \frac{du_{mn}}{d\zeta}(\zeta = 0) \Big/ \frac{du_{00}}{d\zeta}(\zeta = 0). \tag{21}$$

The stress overload in fiber (m,n) is $K_{mn} - 1$.

2.4 Computational effort

Computational effort to implement the above procedure must be expended in obtaining D_{abcd} in Eq. (8) by the sequential application of two fast Fourier transforms (Frigo and Johnson 2005). The asymptotic computational complexity of this operation is $O(\nu^2 \log \nu^2)$. Since $N = \nu^2$, the computational complexity is $O(N \log N)$. Inversion into physical space of the solution given by Eq. (20) using Eq. (11) again costs $O(\nu^2 \log \nu^2)$. It follows that the asymptotic computational cost of the present methodology is $O(N \log N)$.

2.5 Special case: A linear patch

A considerably simpler special case corresponds to the linear array shown in Fig. 1 (b). The $N = \infty$ version of this problem was originally analyzed by Hedgepeth (1961). A periodic patch comprised of $N = \nu$ fibers is considered, with fibers $m = 0$ and $m = \nu - 1$ being considered adjacent to each other. The interaction between fibers can be described by a second-order matrix A_{mp}, which is assumed to obey the translation invariance condition

$$A_{mp} = A_{[m-a],\,[p-a]}, \quad \forall a \in \{0, 1, \ldots, \nu - 1\}. \tag{22}$$

For example, equal interaction of a fiber with its two neighbors,

$$A_{mp} = \begin{cases} -2, & \text{if } p = m, \\ 1, & \text{if } p = [m \pm 1], \\ 0, & \text{otherwise}, \end{cases} \tag{23}$$

satisfies Eq. (22). Eq. (22) implies that A_{mp} is a circulant matrix, which can be directly diagonalized (Rezghi and Eldén 2011, Prop. 4.1) by the Fourier matrix, Eq. (7). In terms of the eigenvalues,

$$\hat{D}_{\alpha\alpha} = \sqrt{\nu} F_{\nu;\alpha m} A_{m0} = \omega_\nu^{\alpha m} A_{m0}, \tag{24}$$

the displacement solution in Fourier space, paralleling Eq. (20), is expressible as

$$\hat{U}_\alpha(\zeta) = \exp\left(-\sqrt{-\hat{D}_{\alpha\alpha}}\zeta\right)/\nu. \tag{25}$$

Details of the derivation follow those in the preceding sections, and are omitted here in the interest of brevity. Paralleling Eq. (21), the stress concentration in fiber m is:

$$K_m := 1 - \frac{du_m}{d\zeta}(\zeta = 0) \Big/ \frac{du_0}{d\zeta}(\zeta = 0). \tag{26}$$

3 Results and discussion

The overloads due to a single break in a rhombus-shaped patch were determined using both the present DFT based method, and the eigenspace method (Landis et al 2000). Both simulations were implemented in the Python language, and run on the same workstation computer. The `Numpy` library was invoked for standard numerical routines in both cases. Using the DFT method, simulations up to $N = 2^{30}$ (approximately one billion fibers) were realized within a few hundred seconds of computer time. It was only possible to simulate much smaller composite patches using the eigenspace method within a reasonable time cap of 10^5 s. The results of both runs, when available, were compared for accuracy, and agreement of stress overloads to 10 decimal places or more was obtained.

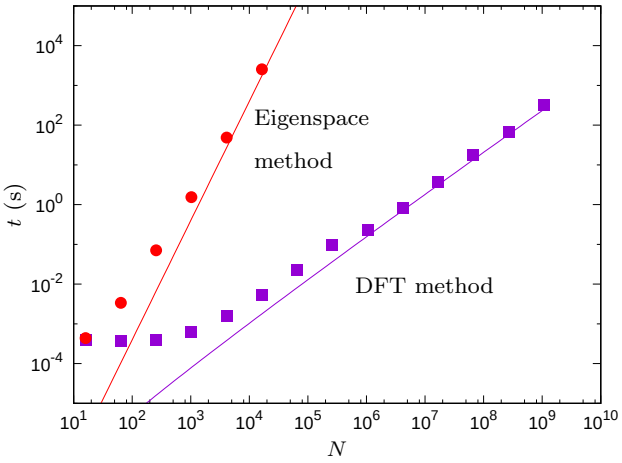

Fig. 2: Scaling of processor time, t, with the number of fibers in the simulation patch N for the eigenspace method of Landis et al (2000) and the present DFT method. The red and violet solid lines indicate $t \sim N^3$, and $t \sim N \log N$, respectively.

Fig. 2 compares the processor times t corresponding to both methods. It is clearly seen that the present method is much faster than the eigensolution based method for all N studied, not just for large N. As expected (Sec. 2.4), at larger N, the processor time using the DFT method approaches $t = 10^{-8} N \log N$, indicated by a solid line in Fig. 2. The processor time using the eigenspace method approaches $t \sim N^3$, also shown in Fig. 2.

The scaling of the stress concentrations with Euclidian distance r from the break is considered next, normalized by the spacing between neighboring fibers in the hexagonal lattice, r_0. The scaling is studied for the rhombus-shaped, and linear patches shown in Fig. 1. Three patch sizes, $N = 2^8$, 2^{14}, and 2^{30}, are considered in each case. Stress concentrations only in the fibers that satisfy $r/r_0 \leq \nu/2$ are shown. In the case of the $N = 2^{30}$ linear patch, however, the stress overloads drop below the computer floating point precision at $r/r_0 = \nu/2$. In this case, therefore, only the overloads greater than the maching precision are shown.

Except when $r/r_0 \approx \nu/2$, the stress overload scales as a power law with Euclidian distance from the break: $K_{mn} - 1 \sim r^{\lambda_\mathrm{r}}$ for the rhombus-shaped patch, and $K_m - 1 \sim r^{\lambda_\mathrm{l}}$, for the linear patch. The power-law exponents, λ_r and λ_l, obtained by fitting, are indicated in the inset tables. It is clear that as $N \to \infty$, $\lambda_\mathrm{r} \to -3$, and $\lambda_\mathrm{l} \to -2$. When $r/r_0 \approx \nu/2$, the influences of the break in the

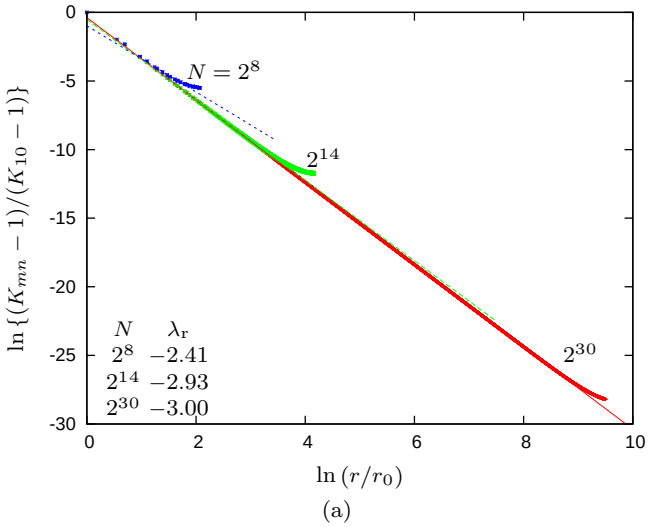

Fig. 3: Power-law scaling of the stress concentration due to a single break with normalized Eucledian distance r/r_0 from the break. r_0 is the distance between two neighboring fibers. Various (a) 2D and (b) 1D patch sizes N have been studied. K_{10} and K_1 denote the stress concentrations in the fibers adjacent to the broken fiber in cases (a) and (b), respectively.

patch and one or more of its periodic images become comparable. This causes the deviation from power-law scaling when $r/r_0 \approx \nu/2$.

The exponent $\lambda_r = -3$ was originally noted by Suemasu (1982), in an infinite composite with a hexagonal lattice. His observation was based on fitting the stress concentrations up to $r/r_0 = 15$. The present method allows the verification of this scaling to much larger $r/r_0 = 2^{14}$. Similarly, the power-law scaling with $\lambda_l = -2$ for the linear patch follows that originally shown analytically by Hedgepeth (1961).

4 Conclusion

A fast $O(N \log N)$ algorithm has been described to determine the overloads in a periodic lattice patch due to a single break. The methodology exploits the circulant structure of the matrix A_{mnpq} describing the interaction between fibers. While the overloads themselves have been computed only for two specific interactions matrices, arbitrary lattices, e.g., Hedgepeth and Van Dyke (1967); Landis et al (1999) that respect the translational invariance conditions, Eq. (4) or Eq. (22), can be addressed by the present method.

Of the two computational challenges associated with performing Monte-Carlo failure simulations in a large patch, numbered (i) and (ii) in Sec. 1, the present solution eliminates the first. The second difficulty, viz., the determination of the overloads in intact fibers by efficiently superposing the single break solution, remains. This latter problem will be addressed in future work.

References

Beyerlein IJ, Phoenix SL, Sastry AM (1996) Comparison of shear-lag theory and continuum fracture mechanics for modeling fiber and matrix stresses in an elastic cracked composite lamina. International Journal of Solids and Structures 33(18):2543–2574

Briggs WL, Henson VE (1995) The DFT: An Owners' Manual for the Discrete Fourier Transform. Society for Industrial Mathematics and Applied Mathematics

Curtin W (1998) Size scaling of strength in heterogeneous materials. Physical Review Letters 80(7):1445

Davis PJ (2012) Circulant matrices. American Mathematical Soc.

De Arcangelis L, Redner S, Herrmann H (1985) A random fuse model for breaking processes. Journal de Physique Lettres 46(13):585–590

Duxbury P, Leath P (1987) The failure distribution in percolation models of breakdown. Journal of Physics A: Mathematical and General 20(6):L411

Frigo M, Johnson SG (2005) The design and implementation of fftw3. Proceedings of the IEEE 93(2):216–231

Habeeb CI, Mahesh S (2015) Strength distribution of planar local load-sharing bundles. Physical Review E 92(2):022,125

Hedgepeth JM (1961) Stress concentrations in filamentary structures. NASA Technical Note,Langley Research Center D-882

Hedgepeth JM, Van Dyke P (1967) Local stress concentrations in imperfect filamentary composite materials. Journal of composite materials 1(3):294–309

Hull D, Clyne T (1996) An introduction to composite materials. Cambridge university press

Landis C, McGlockton M, McMeeking R (1999) An improved shear lag model for broken fibers in composite materials. Journal of composite materials 33(7):667–680

Landis CM, Beyerlein IJ, McMeeking RM (2000) Micromechanical simulation of the failure of fiber reinforced composites. Journal of the Mechanics and Physics of Solids 48(3):621–648

Mahesh S, Phoenix S (2004) Lifetime distributions for unidirectional fibrous composites under creep-rupture loading. International journal of fracture 127(4):303–360

Mahesh S, Beyerlein IJ, Phoenix SL (1999) Size and heterogeneity effects on the strength of fibrous composites. Physica D: Nonlinear Phenomena 133(1):371–389

Mahesh S, Phoenix SL, Beyerlein IJ (2002) Strength distributions and size effects for 2d and 3d composites with weibull fibers in an elastic matrix. International Journal of Fracture 115(1):41–85

Newman WI, Gabrielov AM, Durand TA, Phoenix SL, Turcotte DL (1994) An exact renormalization model for earthquakes and material failure statics and dynamics. Physica D: Nonlinear Phenomena 77(1-3):200–216

Rezghi M, Eldén L (2011) Diagonalization of tensors with circulant structure. Linear Algebra and its Applications 435(3):422–447

Smith RL (1980) A probability model for fibrous composites with local load sharing. In: Proceedings of the Royal Society of London A: Mathematical, Physical and Engineering Sciences, The Royal Society, vol 372, pp 539–553

Suemasu H (1982) An analytical study of probabilistic aspects of strength of unidirectional fiber reinforced composites under tensile loads. Japan Society for Composite Materials, Transactions 8:29–36

Zhou S, Curtin W (1995) Failure of fiber composites: a lattice green function model. Acta Metallurgica et Materialia 43(8):3093–3104